ELSEVIER

Chemical Engineering Journal 76 (2000) 33–47

Chemical Engineering Journal

www.elsevier.com/locate/cej

Comparison of equilibrium stage and nonequilibrium stage models for reactive distillation

R. Baur [a,b], A.P. Higler [a,b], R. Taylor [b], R. Krishna [a,*]

[a] *Department of Chemical Engineering, University of Amsterdam, Nieuwe Achtergracht 166, 1018 WV Amsterdam, Netherlands*

[b] *Department of Chemical Engineering, Clarkson University, Potsdam, NY 13699-5705, USA*

Received 18 March 1999; received in revised form 15 July 1999; accepted 27 July 1999

Abstract

For modelling reactive distillation columns, two distinctly different approaches are available in the literature: (1) the equilibrium (EQ) stage model, in which the vapour and liquid phases are assumed to be in thermodynamic equilibrium, and (2) the nonequilibrium (NEQ) stage model in which the finite mass transfer rates across the vapour–liquid interface are accounted for. In this paper, these two approaches are compared using two case studies: (a) synthesis of MTBE and (b) hydration of ethylene oxide to ethylene glycol. It is shown that while the phenomena of multiple steady states is exhibited by both modelling approaches, the "window" in which these multiplicities occur is significantly reduced in the NEQ model. It is also shown that in actual column design, some of the steady states calculated by the EQ model cannot be realised due to e.g. flooding or weeping limitations on distillation trays. Another important conclusion that can be drawn from this work is that the hardware design can have a significant influence on the conversion and selectivity. It is concluded that for design of reactive distillation columns we must adopt the NEQ modelling approach.

Keywords: Reactive distillation; Equilibrium stage model; Nonequilibrium stage model; Multiple steady states; Maxwell–Stefan equations; Methyl *tert*-butyl ether synthesis; Ethylene glycol; Tray design

Nomenclature

a	interfacial area (m^2)
c	number of components (dimensionless)
c_t	total concentration ($mol\,m^{-3}$)
$D_{i,k}$	Maxwell–Stefan diffusivity ($m^2\,s^{-1}$)
E	energy transfer rate ($J\,s^{-1}$)
F^V	vapour feedstream ($mol\,s^{-1}$)
F^L	liquid feedstream ($mol\,s^{-1}$)
f	component feed stream ($mol\,s^{-1}$)
h_{cl}	clear liquid height (m)
h_w	weir height (m)
H	molar enthalpy ($J\,mol^{-1}$)
h	heat transfer coefficient ($W\,m^{-2}\,K^{-1}$)
K	vapour–liquid equilibrium constant (dimensionless)
L	liquid flow rate ($mol\,s^{-1}$)
L_M	interchange liquid flow rate between horizontal rows of cells in Fig. 3 ($mol\,s^{-1}$)
N	mass transfer rate ($mol\,s^{-1}$)
p_j	stage pressure (Pa)
Q	heat duty ($J\,s^{-1}$)
Q_L	liquid flow rate across tray ($m^3\,s^{-1}$)
$R_{m,j}$	reaction rate ($mol\,m^{-3}\,s^{-1}$)
R	gas constant ($J\,mol^{-1}\,K^{-1}$)
r	number of reactions (dimensionless)
T	temperature (K)
V	vapour flowrate ($mol\,s^{-1}$)
W	weir length (m)
x	mole fraction in the liquid phase (dimensionless)
y	mole fraction in the vapour phase (dimensionless)

Greek symbols

ε	reaction volume (m^3)
η	dimensionless coordinate (dimensionless)
κ	mass transfer coefficient ($m\,s^{-1}$)
μ	chemical potential ($J\,mol^{-1}$)
ν	stoichiometric coefficient (dimensionless)

Subscripts

i	component index
j	stage index
k	alternative component index
m	reaction index
t	total

Superscripts

F	referring to feed stream
I	referring to interface

* Corresponding author. Tel.: +31-20-525-7007; fax: +31-20-525-5604
E-mail address: krishna@chemeng.chem.uva.nl (R. Krishna)

1385-8947/00/$ – see front matter
PII: S1385-8947(99)00114-X

L referring to liquid phase
V referring to vapour phase

1. Introduction

Currently there is considerable academic and industrial interest in multifunctional reactors, involving in situ separation of products from the reactants [30]. Reactive distillation is one of the most common means of in situ product removal and has been receiving increasing attention in recent years as an alternative to the conventional reaction-followed-by-distillation processes [2,12,13,17,54]. Doherty and Buzad [13] have placed this subject in historical perspective and list references to show that the advantages of reactive distillation were recognised as early as in 1921. Reactive distillation is potentially attractive whenever a liquid phase reaction must be carried out with a large excess of one reactant. Under such circumstances, conventional processes incur large recycle costs for excess reactant. Reactive distillation, on the other hand can be carried out closer to stoichiometric feed conditions, thereby eliminating recycle costs. Both homogeneous and heterogeneous catalysed chemical reactions can be carried out in a reactive distillation column.

There are four potential benefits of reactive distillation operation:

1. Higher conversions are obtained for equilibrium-limited reactions due to shifting of the equilibrium to the right. This is exemplified by the production of methyl acetate [2,51], methyl-*tert* butyl ether, MTBE [53], *tert*-amyl ether [6] and production of condensation polymers [19].
2. In some applications, chemical reaction has the beneficial effect of "reacting away" some of the azeotropes in the mixture and greatly simplifying the phase equilibrium behaviour. This happens in the process for synthesis of MTBE.
3. Improved selectivity is obtained because of removal of products from the reaction zone and preventing these from undergoing further reaction to by-products. Such benefits are obtained for example in the production of propylene oxide from propylene chlorohydrins [7,8], for the alkylation of benzene to produce cumene [50] and alkylation of butane to isooctane.
4. Benefits of heat integration are obtained because the heat generated in the chemical reactions is used for vaporisation. This is particularly advantageous for situations involving high heats of reaction such the hydration of ethylene oxide to ethylene glycol [9]. Hot spot formation is therefore prevented.

A typical set-up used for reactive distillation is shown in Fig. 1. A column usually is split up in three sections: a reactive section, in which the reactants are converted into products and where, by means of distillation, the products are separated out of the reactive zone. The tasks of the rectifying and stripping sections depend on the boiling points of reactants and products. If the product is the lowest boiling component in the process, the rectifying section is used for product purification and reactant recycle, and the stripping section mainly for inert and by-product removal as well as reactant recycle. In case the product is the highest boiling component, the tasks of the rectifying and stripping sections are switched. With the set-up as shown in Fig. 1, it is possible to virtually eliminate an entire post processing train in a process. One of the most spectacular examples of this kind is the Eastman process for production of methyl acetate [51].

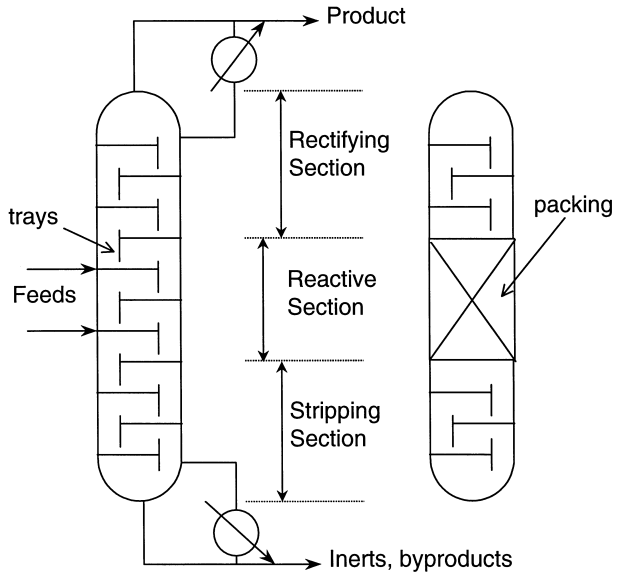

Fig. 1. Typical configuration of a reactive distillation tray column consisting of three sections: (a) rectifying section, (b) reactive section and (c) stripping section.

The design and operation issues for reactive distillation systems are considerably more complex than those involved for either conventional reactors or conventional distillation columns. The introduction of an in situ separation function within the reaction zone leads to complex interactions between vapour–liquid equilibrium, vapour–liquid mass transfer, intra-catalyst diffusion (for heterogeneously catalysed processes) and chemical kinetics. Such interactions have been shown to lead the phenomenon of multiple steady states and complex dynamics, which have been verified in experimental laboratory and pilot plant units [6,37,41].

For carrying out homogeneous reactions in reactive distillation columns, either trays or structured packings can be used. The hardware design is dictated by considerations other than that for conventional distillation. This is because when we carry out a reaction in the liquid phase, the liquid phase residence time distribution has a significant impact on the conversion and selectivity. The liquid phase residence time distribution is much less important for conventional distillation. For heterogeneously catalysed processes, hardware design poses considerable challenges. The catalyst particle sizes used in such operations are usually in the 1–3 mm range. Counter-current operation in fixed beds packed with such particles is difficult because of flooding limitations. To

overcome the limitations of flooding the catalyst particles have either to be enveloped in wire gauze [4,15,26,60] or the packing itself made catalytically active [55].

For design of reactive distillation columns, we require a model. Broadly speaking, two types of modelling approaches have been developed in the literature: the equilibrium (EQ) stage model and the nonequilibrium (NEQ) stage model. In the EQ stage model the vapour and liquid phase are assumed to be in equilibrium and allowance is made for finite reaction rates [1,3,7–9,14,16,22,27,38,40,45,47,48,52]. Such models stem from conventional equilibrium-stage modelling of distillation columns [49].

The NEQ stage model for reactive distillation follows the philosophy of rate based models for conventional distillation [32,49,58]. The description of the interphase mass transfer, in either fluid phase, is almost invariably based on the rigorous Maxwell–Stefan theory for calculation of the interphase heat and mass transfer rates [6,23–25,29,35,46, 53,55,61].

In the literature, there has also been considerable attention to the phenomena of multiple steady states. Using the EQ stage model, steady-state multiplicities have been reported for applications such as synthesis of MTBE [20–22,27,37,38], synthesis of ETBE [56], synthesis of TAME [37,41] and for production of ethylene glycol [9,34]. Schrans et al. [48] and Kumar and Daoutidis [34] have performed dynamic simulations using the EQ stage approach to show the rich dynamic features of reactive distillation columns. For example, it has been shown by Schrans et al. [48] for MTBE synthesis, that small perturbation of reactant feed to the column could trigger oscillations and could shift the column operation from one steady state with high conversion to another steady state, with a significantly reduced conversion.

The objective of this paper is to compare the EQ and NEQ modelling of reactive distillation columns, focusing on the phenomena of multiple steady states. The column hardware design (column diameter, tray configuration, size and configuration of packing, etc.,) will have a significant influence on the interphase heat and mass transfer rates which are not taken account of in the EQ stage model. We examine the extent to which column hardware design influences the "window" within which multiple steady states are experienced. Two different case studies are undertaken, MTBE synthesis and production of ethylene glycol.

2. Nonequilibrium model development

A schematic representation of the NEQ model is shown in Fig. 2. This NEQ stage may represent a tray or section of packing. The development of the material balances, component balances, interphase transport equations and reaction rate equations are the same as developed in our earlier papers [23–25]. Our model formulation can deal with any number of reactions and the component molar balances for

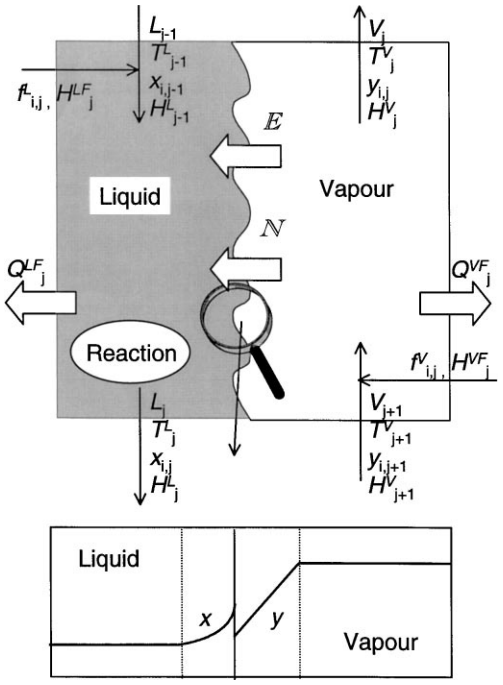

Fig. 2. Schematic representation of the nonequilibrium model describing interphase mass transfer, with liquid phase chemical reaction at a position in a tray or packed column. The NEQ model takes account of the enhancement of the mass transfer due to chemical reaction within the diffusion film in the liquid close to the interface (see inset).

the vapour and liquid phases are

$$V_j y_{i,j} - V_{j+1} y_{i,j+1} - f^{\mathrm{V}}_{i,j} + \mathbf{N}^{\mathrm{V}}_{i,j} = 0, \tag{1}$$

$$L_j x_{i,j} - L_{j-1} x_{i,j-1} - f^{\mathrm{L}}_{i,j} - \mathbf{N}^{\mathrm{L}}_{i,j} - \sum_{m=1}^{r} \nu_{i,m} R_{m,j} \varepsilon = 0, \tag{2}$$

where $\mathbf{N}_{i,j}$ is the interfacial mass transfer rate and $R_{m,j}$ is the rate of reaction m on stage j. $\nu_{i,m}$ represents the stoichiometric coefficient of component i in reaction m and ε_j represents the reaction volume. For homogeneous reactions this is given by the total liquid holdup on stage j. For heterogeneous reactions, employing the pseudo-homogeneous description, this is given by the total amount of catalyst present on the stage under consideration. The overall molar balances are obtained by summing Eqs. (1) and (2) over the total number (c) of components in the mixture. The $\mathbf{N}_{i,j}$ are related to the chemical potential gradients in either phase by the generalised Maxwell–Stefan equations [31,58].

$$\frac{x_{i,j}}{\mathbf{R}T_j} \frac{\partial \mu^{\mathrm{L}}_{i,j}}{\partial \eta} = \sum_{k=1}^{c} \frac{x_{i,j}\mathbf{N}^{\mathrm{L}}_{k,j} - x_{k,j}\mathbf{N}^{\mathrm{L}}_{i,j}}{c^{\mathrm{L}}_{t,j}\left(\kappa^{\mathrm{L}}_{i,k} a\right)_j} \tag{3}$$

with a similar relation for the vapour phase. The $\kappa^{\mathrm{L}}_{i,k}$ represents the mass transfer coefficient of the i–k pair in the

liquid phase; this coefficient is estimated from information on the corresponding Maxwell–Stefan diffusivity $D_{i,k}$ using the standard procedures discussed in [58]. Only $c-1$ of Eq. (3) are independent. The mole fraction of the cth component is obtained by the summation equations for both phases. The enthalpy balances for both vapour and liquid phase are

$$V_j H_j^{\mathrm{V}} - V_{j+1} H_{j+1}^{\mathrm{V}} - F_j^{\mathrm{V}} H_j^{\mathrm{VF}} + \mathbf{E}_j^{\mathrm{V}} + Q_j^{\mathrm{V}}, \tag{4}$$

$$L_j H_j^{\mathrm{L}} - L_{j-1} H_{j-1}^{\mathrm{L}} - F_j^{\mathrm{L}} H_j^{\mathrm{LF}} - \mathbf{E}_j^{\mathrm{L}} + Q_j^{\mathrm{L}}, \tag{5}$$

where the interphase energy transfer rates $\mathbf{E}_j$ (equal in both phases) have conductive and convective contributions

$$\mathbf{E}_j^{\mathrm{L}} = -h_j^{\mathrm{L}} a \frac{\partial T^{\mathrm{L}}}{\partial \eta} + \sum_{i=1}^{c} \mathbf{N}_{i,j}^{\mathrm{L}} H_{i,j}^{\mathrm{L}} \tag{6}$$

with a similar relation for the vapour phase. h_j^{L} is the heat transfer coefficient in the liquid phase.At the vapour liquid interface we assume phase equilibrium

$$y_{i,j}^{\mathrm{I}} - K_{i,j} x_{i,j}^{\mathrm{I}} = 0, \tag{7}$$

where the superscript I denotes the equilibrium compositions and $K_{i,j}$ is the vapour–liquid equilibrium ratio for component i on stage j.

In addition to qs. (1–7, we have the summation equations for the mole fractions in the vapour and liquid phase and equations expressing the continuity of fluxes of mass and energy across the interface. Furthermore, in the NEQ model we take account of the pressure drop across a stage

$$p_j - p_{j-1} - \left(\Delta p_{j-1}\right) = 0, \tag{8}$$

where p_j and p_{j-1} are the stage pressures and Δp_{j-1} is the pressure drop per tray from stage $(j-1)$ to stage j. The pressure drop over the stage is considered to be a function of the stage flows, the physical properties and the hardware design.

In the NEQ model, hardware design information must be specified so that mass transfer coefficients, interfacial areas, liquid hold-ups can be calculated. The NEQ model requires thermodynamic properties, not only for calculation of phase equilibrium but also for calculation of driving forces for mass transfer and, in reactive distillation, for taking into account the effect of nonideal component behaviour in the calculation of reaction rates and chemical equilibrium constants. In addition, physical properties such as surface tension, diffusion coefficients, viscosities, etc. for calculation of mass (and heat) transfer coefficients and interfacial areas are required. A list of property models and mass transfer correlations available in our program is provided in Table 1. For most part, the property models are those recommended by Reid et al. [44] and by Dannner and Daubert [11]. The details of the models used for estimation of diffusivities and mass transfer coefficients are discussed in standard texts [36,49,58]. The tray design procedure is discussed in detail in [28,57]. Interested readers can download the technical manual from the ChemSep website: http://www.clarkson.edu/~chengweb/faculty/taylor/chemsep/chemsep.html, which contains details of all thermodynamics, hydrodynamics and mass transfer models for tray and packed columns which have already been implemented into our reactive distillation software. The code for these models represents a large fraction of the overall program size.

For each reaction, we need to know the stoichiometric coefficients, reaction orders, and kinetic constants and whether the reaction is heterogeneous or homogeneous. A homogeneous reaction can also take place in the mass transfer film, the modelling of which requires additional equations for taking into account the effect of the reaction on the interphase mass transfer rate. Finally, we need to know the reaction volume. In EQ model simulations, the reaction volume often is specified. In the NEQ model, is the reaction volume equal to the total liquid hold-up on a stage; this is obtained directly from the packing specifications and hydrodynamic correlations. For a heterogeneous reaction, there are two options for the description of the reaction term. The simplest way is to treat the reaction pseudo-homogeneously, whereby catalyst diffusion and reaction is lumped into an overall reaction term. In this case, one only needs to specify catalyst weight and activity. This approach is adopted here. A more rigorous approach would involve a more detailed description of diffusion and reaction inside the catalyst particles; see for example, [53]. In this case one also needs information about the catalyst geometry (surface area, mean pore diameter, etc).

The steady-state model equations are solved using Newton's method as outlined in [57]. In addition, we have equipped the program with a continuation method for analysis of multiple steady state behaviour. For more details about this method, the reader is referred to [33,59].

A further aspect that needs to be considered concerns the modelling of the residence time distribution of the vapour and liquid phases on any "stage". If the column with random dumped or structured packings, it is reasonable to assume that the vapour and liquid phases at any horizontal slice is in true *counter-current* (plug) flow. The situation with respect to vapour–liquid contacting on trays is significantly different. The contacting pattern on any tray, i.e. stage, is *cross-flow* of the vapour and liquid phases. Depending on the flow regime (froth or spray), dispersion height, and liquid flow path length, each phase (vapour or liquid) could be considered to be in plug flow, well mixed or have a mixing characteristics in between these extremes. Since the residence times and residence time distributions of the liquid and vapour phase can severely affect the performance of a reactor, it is important to develop a proper model to handle these extremes. For this purpose, we have adopted the multiple-cells-per-stage approach, see Fig. 3. In this more

Table 1
Thermodynamic, physical property and mass transfer models incorporated into the reactive distillation design program

K-value models	*Enthalpy*
Raoult's law	None
Equation of state	Ideal
Gamma–Phi	Ideal + excess (from EOS or activity model)
Chao–Seader	
Polynomial	
Equations of state	*Activity coefficients*
Ideal gas	Ideal solution
Virial	Scatchard–Hildebrand
Redlich–Kwong	Margules
Soave–Redlich–Kwong	Van Laar
API–SRK	Wilson
Peng–Robinson	NRTL
	UNIQUAC
	UNIFAC
	ASOG
Molar volume	*Vapour pressure*
EOS based methods	Antoine
Rackett equation	Extended Antoine
Yen–Woods	DIPPR polynomial
Thompson–Probst–Hankinson	Riedel
Amagat's law	Lee–Kesler
	Cubic EOS
Viscosity	*Thermal conductivity*
DIPPR polynomial (gases and liquids)	DIPPR polynomial (gases and liquids)
Chapman–Enskog–Brokaw (gases)	Misic–Thodos (gases)
Brokaw (gas mixtures)	Stiel–Thodos (gases)
Yoon–Thodos (gases)	API procedure 12A1 (liquids)
Letsou–Stiel (liquid mixtures) DIPPR procedure 8H	DIPPR procedure 9I (liquid mixtures)
	DIPPR procedure 9B (gases)
	Wassiljewa–Mason–Saxena (gas mixtures)
	DIPPR procedure 9E (liquids)
	DIPPR procedure 9H (liquid mixtures)
Surface tension	*Binary diffusion coefficients*
DIPPR polynomial	Kinetic theory (gases)
Lielmezs–Herrick	Fuller–Schettler–Giddings (gases)
API method	Wilke–Change (dilute liquids)
Brock–Bird	Hayduk–Laudie (dilute liquids)
Digulio–Teja	Hayduk–Minhas (dilute liquids)
McLeod–Sugden	Siddiqi–Lucas (dilute liquids)
Winterfield–Scriven–Davis	Generalized Vignes (liquid mixtures)
	Leffler–Cullinan (liquid mixtures)
	Rathbun–Babb (liquid mixtures)
Mass transfer coefficients — packings	*Mass transfer coefficients — trays*
Onda et al.	AIChE method
Bravo–Fair	Hughmark
Billet Schultes	Chan–Fair
Sherwood number correlation	Zuiderweg
Bravo–Rocha–Fair (1985)	Harris
Bravo–Rocha–Fair (1992)	Chen–Chuang
Zogg	
Brunazzi	
Ronge	
Zogg–Toor–Marchello	

recent development, each stage is considered to be made up of multiple cells in either fluid phase, (see Fig. 3, [25]). The vapour–liquid dispersion on a tray is split up in several cells within which interphase mass transfer and subsequent chemical reactions occur. For each of these cells we can write a set of equations as presented above for a single stage. Various forms of mixing behaviour can now be modelled by specifying a number of cells in the direction of flow of the vapour and liquid phases. Literature correlations are available to determine these mixing characteristics

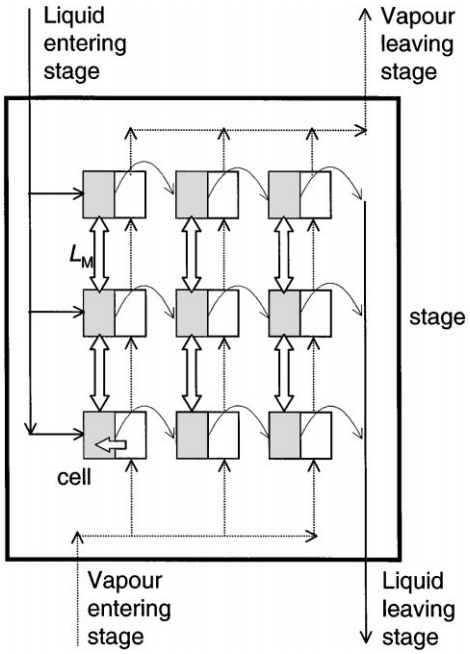

Fig. 3. Schematic of the nonequilibrium cell model. For details of the NEQ cell model see [25].

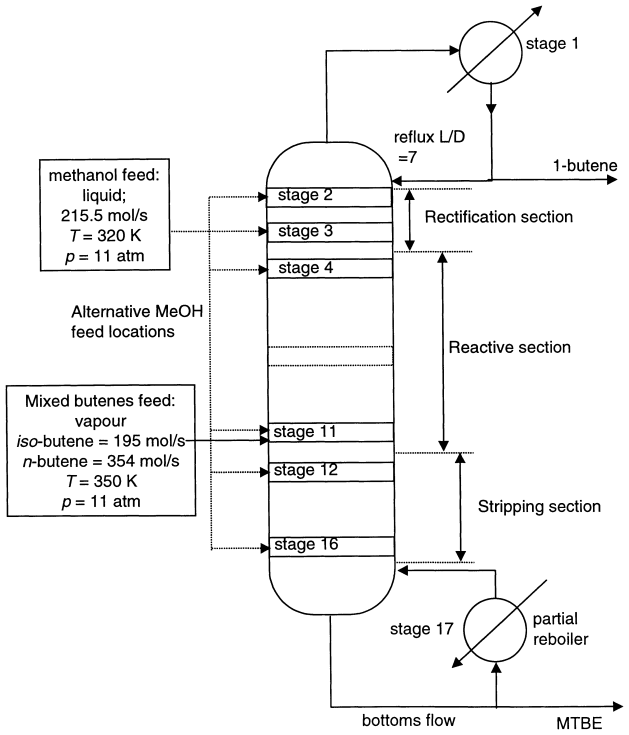

Fig. 4. Configuration of the MTBE synthesis column, following [27]. The column consists of 17 stages.

[5,18]. By varying the number of cells in a flow path we can go from a perfectly mixed phase on a stage (1 cell per flow path), to an approximation of plug flow (large number of cells, typically more than 4). To make the multi-cell model complete we need to specify the interchange of liquid (with a molar flow rate of L_M) between horizontal rows of cells; this interchange is denoted by double headed arrows in Fig. 3. In setting up the proper component and enthalpy balances for the multi-cell model we need to take the following considerations into account.

- The amount of liquid entering a cell from the cell above (below) is exactly the same as the amount of liquid leaving the cell to the cell below (above).
- The liquid mixing flow L_M is large as compared to the flow of the liquid entering and leaving each cell.

In practice the vapour jet issuing from the holes on a tray will create a "fountain" effect; this will tend to mix the liquid phase more or less completely in the vertical direction [36,62]. In order to model this situation in which the liquid compositions in any vertical column of cells have the same composition, we choose a value of L_M which is considerably larger, say 10 times, than the liquid flow on that stage. In all the calculations presented in this paper involving tray internals, the liquid phase in a vertical column of cells is assumed to be well mixed.

Two special versions of the NEQ model formulation were derived as special cases. In the EQ version, the vapour and liquid phases were assumed to be in thermodynamic equilibrium. Another special version of the NEQ model was prepared, called the equal diffusivities NEQ model, in which the Maxwell–Stefan diffusivities in either fluid phase, $D_{i,k}$, equal one another.

3. MTBE case study

The column configuration chosen for the simulations is shown in Fig. 4; this is the configuration described by Jacobs and Krishna [27] in their simulation study using the EQ stage model. The total number of stages is 17, including a total condenser and a partial reboiler; the column pressure is 11 atm. Reactive stages are located in the middle of the column, stage 4 down to and including stage 11. The column has two feed streams: a methanol feed and a mixed butenes feed. A small stoichiometric excess of methanol is used. The methanol feed stage location is varied in the simulations between stage 2 and stage 16. The mixed butenes feed, to stage 11, contains a mixture of *iso*-butene, which is reactive, and *n*-butene, which is nonreactive or inert. The reflux-ratio is set to 7 and the bottom flow rate is either set to 203 mol s^{-1} or varied (as a continuation parameter). The product removed from the top of the column is predominantly the inert *n*-butene. The bottoms product consists predominantly of MTBE. For a properly designed and operated column it is possible to achieve close to 100% conversion of *iso*-butene.

On each of the eight stages in the reactive zone, 1000 kg of catalyst is introduced. The total amount of catalyst in the reactive zone is 8000 kg. For NEQ model calculations, it is necessary to further specify the hardware configurations. In this study the reactive section is taken to be packed with catalytically active packing material in the form of Raschig rings. Specifically, we use 1/4 in. Raschig ring

Table 2
Tray specifications for the rectifying and stripping sections in the MTBE column

	Rectifying section	Stripping section
Type of tray	Sieve	Sieve
Column diameter (m)	5.595	5.019
Total tray area (m^2)	24.58	19.78
Number of liquid flow passes	5	5
Tray spacing (m)	0.61	0.61
Liquid flow path length (m)	0.92	0.82
Active area (m^2)	19.21	15.32
Total hole area (m^2)	2.12	1.52
Downcomer area (m^2)	2.68	2.23
Hole diameter (m)	0.0047625	0.0047625
Weir length (m)	22.95	20.62
Weir height (m)	0.0508	0.0508
Weir type	Segmental	Segmental
Downcomer clearance (m)	0.0381	0.0381
Deck thickness (m)	0.00254	0.00254

shaped ion-exchange (Amberlyst 15) catalyst packing as described by Sundmacher and Hoffmann [54]. The specifications of the reactive section are: column diameter = 6 m, reactive packed zone height = 0.7 m, specific packing surface = 600 $m^2\,m^{-3}$, void fraction in the column = 0.72, packing density = 410 $kg\,m^{-3}$, catalyst pore voidage = 0.45, ion-exchange capacity of catalyst = 4.54 (meq H^+/g). The nonreactive rectifying and stripping sections are configured as sieve trays. The design specifications are given in Table 2.

The UNIQUAC model was used for description of liquid phase nonideality, while the Soave–Redlich–Kwong equation of state was used for the vapour phase. The extended Antoine equation was used for calculation of the vapour pressure. Thermodynamic and kinetic data are taken from [42,43].

The basic objective of this paper is to compare the results of EQ and NEQ models. The separation capability of the nonreactive stripping and rectifying sections will also affect the overall column performance. We decided to focus on the differences of the EQ and NEQ modelling of the reactive section only, and therefore, assumed the nonreactive stages to have equal separation capability in both implementations. Towards this end, in the EQ model implementation we have assumed a tray efficiency of 60% for the nonreactive stages; this value corresponded closely to the calculations of the NEQ model for the nonreactive stripping and rectifying sections using the *AIChE* calculation method for sieve tray mass transfer (for details of this model see [36]). Of course, in the NEQ model implementation of the nonreactive stages, stage efficiencies are not used in the calculations but can be calculated from the simulation results; these stage efficiencies vary for individual components. For the reactive section, the EQ model assumes vapour and liquid phases to be in equilibrium. In the NEQ model for the reactive section the mass transfer coefficients are calculated using the Onda et al. [39] correlation. The 0.7 m high packed reactive section needs to be divided into a sufficient number of "slices" for accurate calculations. Our study shows that at least 90 slices are required for acceptable accuracy. Increasing the number of slices beyond 90 does not alter the results.

A series of simulation runs were carried out with varying methanol feed stage location; the methanol feed is moved sequentially down the column from stage 2 to stage 16 and up again. Once a run is completed successfully, different cases are generated by slightly altering the specifications and initiating the calculations using the previously obtained, converged, results. Fig. 5(a) compares the *iso*-butene conversions for the EQ and NEQ models with varying methanol feed stage locations. Consider the simulations of the EQ model first. Moving the methanol feed down the column from stage 2 to stage 11 gives a series of solutions that correspond to high (90% +) conversion. When the feed is moved one stage further, i.e. to stage 12, a sharp decrease in conversion is observed. A series of low conversion solutions is found moving the methanol feed from stage 12 to stage 16. Starting at stage 16 the methanol feed is moved upward. Until stage 12, the solutions for the up- and down-going sequences are identical. Continuing the up-going sequence beyond stage 12, does not give the expected jump back to the high conversion level but a different set of solutions is found. Thus, a set of low conversion solutions is found when methanol is fed to trays 11 or 10. The above results are largely in agreement with the simulations of Jacobs and Krishna [27] which were performed with the commercial software RADFRAC of Aspen Technology, USA.

The calculations using the NEQ model are also shown in Fig. 5(a) as continuous curves. The differences in conversion between the high conversion branches of the EQ and NEQ models are small. Moving the methanol feed from stage 11 to stage 12 results in a jump to a lower conversion level, but this jump is much smaller than for the EQ model. A further difference between the EQ and NEQ models is that we did not observe any hysteresis effect for the NEQ model and moving the methanol feed from stage 12 to stage 11 results in a high conversion steady state.

The results of Fig. 5(a) are counter-intuitive in that introduction of mass transfer resistance (in the NEQ model) results in a higher conversion for methanol feed introduction between stages 11 and 16. To underline this counter-intuition we also carried out NEQ model simulations to study the sensitivity of the NEQ model to variations in the interphase mass transfer coefficients, 110% and 90% of the base case; these simulations are shown in Fig. 5(b). It is interesting to note that when the mass transfer coefficient is increased to 110%, the *iso*-butene conversion decreases for the low-conversion branch. When the mass transfer coefficient is decreased to 90% of the base case value, the conversion of the low-conversion branch increases. Increase or decrease in the mass transfer coefficients does not affect the high-conversion branch to any significant extent (in fact the conversion values correspond closely to that of the EQ model). For the 90% mass transfer coefficient simulation, the NEQ model calculations show no conversion jump and

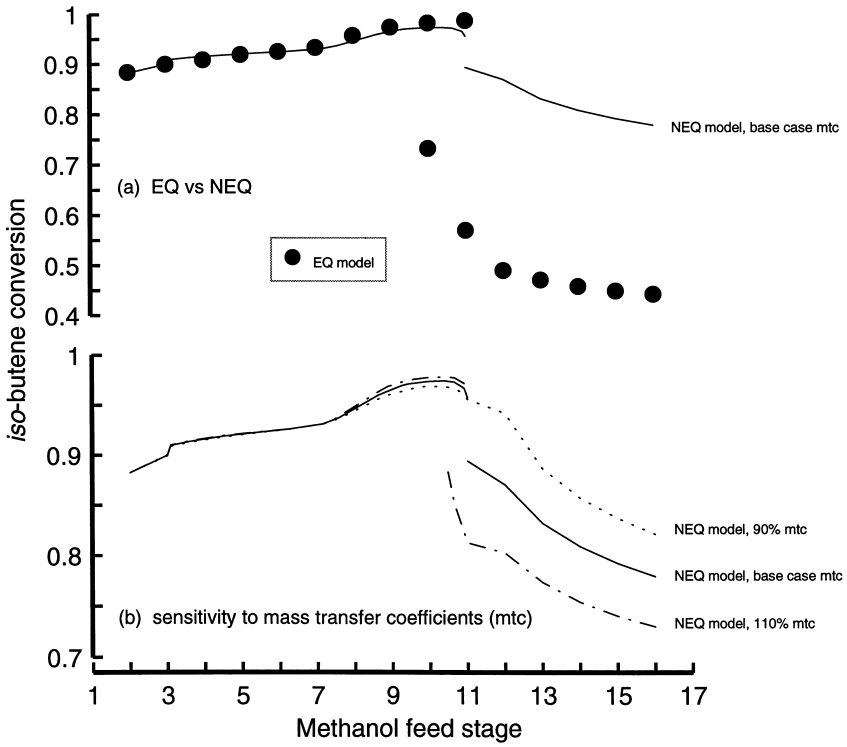

Fig. 5. (a) High and low conversion branches obtained by EQ and NEQ simulations for the configuration shown in Fig. 4. The bottom flows in these simulations were fixed at 203 mol s^{-1}. (b) NEQ simulations to study the sensitivity to mass transfer coefficients. The three curves represent (1) base case, (2) mass transfer coefficients increased to 110% of base case and (c) mass transfer coefficients reduced to 90% of base case.

yields a continuous smooth line over the whole range of stages to which methanol is injected.

In order to understand this counter-intuitive effect, let us consider the specific simulation in which the methanol is fed to stage 11. For this simulation, the *iso*-butene consumption rates are plotted along the height of the packed reactive section in Fig. 6. Fig. 6(a) and (b) show the calculations for the high conversion branch and low conversion branches, respectively. Also plotted in Fig. 6 are the interphase mass transfer rates calculated from the NEQ model (for the EQ model, the mass transfer coefficients are infinitely large, leading to phase equilibrium). Examination of Fig. 6(b) shows that in the EQ model the reaction is proceeding in the reverse direction (reaction of MTBE to *iso*-butene and methanol) in the bottom half of the reactive section; this is evidenced by the fact that the *iso*-butene consumption rate is negative. This is clearly an undesirable situation. Introduction of mass transfer resistance (as is done in the NEQ model) hinders this. The counter-intuitive effect observed in Fig. 5(a) is because in the low conversion branch the reaction is proceeding in the "wrong" direction and decreasing the interphase transfer facility helps by mitigating a bad situation.

Furthermore when we compare the mass transfer rates with the *iso*-butene consumption rates, we see from Fig. 6(a) and (b) that for the high-conversion branch the mass transfer rates are considerably higher than the consumption rates and mass transfer is not a limiting factor. This explains why increase or decrease in the mass transfer coefficient in this high conversion-branch does not affect the conversion level, as observed in Fig. 5(b). For the low-conversion branch, on the other hand, the *iso*-butene consumption rates are very close to the mass transfer rates. For this case, therefore, the mass transfer coefficient has a significant influence on the conversion. Furthermore, at the bottom of the reactive section the reaction is proceeding in the "wrong" direction; introduction of more mass transfer resistance is helpful. This also explains why increase in the mass transfer coefficient decreases the conversion of *iso*-butene for the low conversion branch (cf. Fig. 5(b)).

In the dynamic simulation study of Scharans et al. [48], using the EQ model, it was shown that a small perturbation in the concentration of either methanol or *iso*-butene feed to the column could trigger oscillations, and perhaps, a shift in operation from the high conversion branch to the lower conversion branch. It should be clear from the results of Fig. 5 that in practice, where we do have interphase mass and heat transfer resistances, the oscillations would be much smaller in magnitude and the conversion jumps would be much less severe than anticipated by the EQ model. In order to stress the point we have carried out simulations using the EQ and NEQ model with the bottoms flow rate as continuation parameter. For methanol feed to stage 11, Fig. 7 shows the bifurcation diagrams for the EQ and NEQ models. It is clear that

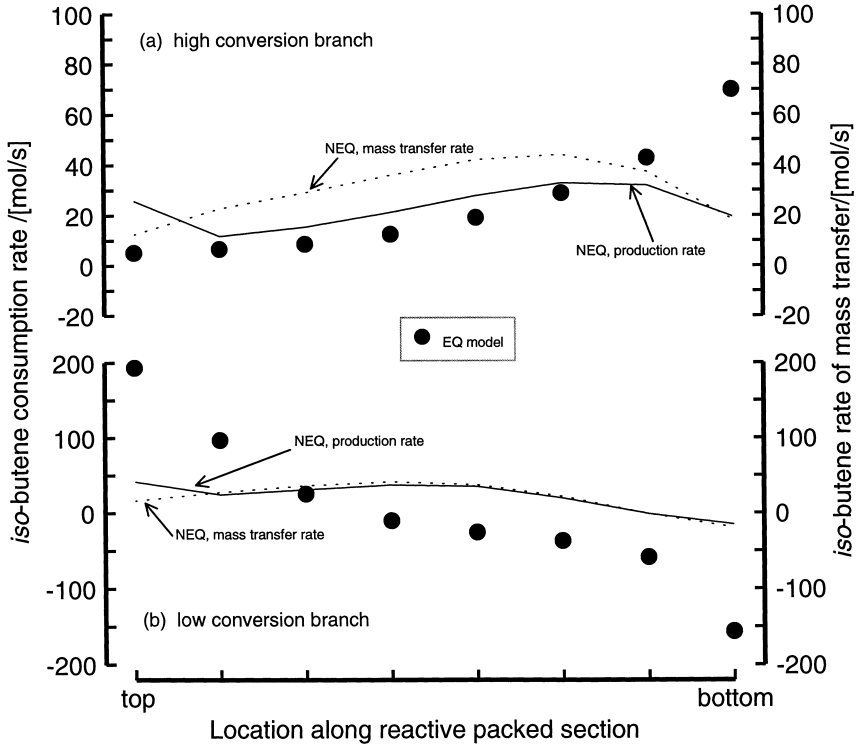

Fig. 6. The *iso*-butene consumption rates for the (a) high and (b) low conversion branches obtained by EQ and NEQ simulations for the configuration shown in Fig. 4. The bottom flows in these simulations were fixed at 203 mol s^{-1}. For the NEQ simulations, the interphase mass transfer rates are also plotted for the high and low conversion steady states.

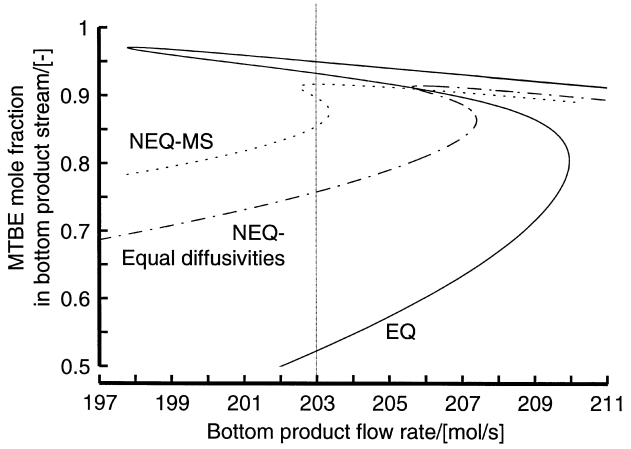

Fig. 7. Bifurcation diagram for the EQ and models NEQ (both Maxwell–Stefan and equal diffusivities) with the bottoms product flow rate as continuation parameter. In these simulations the methanol feed is to stage 11 of the column configuration shown in Fig. 4.

the "window" within which steady-state multiplicity is observed is much narrower with the NEQ model. Furthermore, the "downside" scenario (i.e. lower conversion branch operation) is much less bleak. This would suggest that the phenomena of multiple-steady states gets exaggerated attention if we use the EQ model. Also drawn in Fig. 7 are the results of the NEQ model calculations in which the diffusivities of the species are forced to equal one another in either fluid phase. We see that for a bottom flow rate of 203 mol s^{-1}, the equal diffusivities model exhibits only the low conversion steady-state whereas both the EQ and NEQ model (with the complete Maxwell–Stefan formulation), each predict three steady-states. For the low-conversion branch the *iso*-butene conversion with the equal diffusivities model is lower than that of the NEQ Maxwell–Stefan model because the latter model takes proper account of the fact that the facility for transfer of MTBE should be lower than that of the other species. This reduced facility of MTBE transfer helps to prevent the backward reaction of MTBE to the reactants. Clearly, a proper modelling of mass transfer phenomena is essential in describing the phenomena of multiple steady-states and column dynamics.

4. Ethylene glycol case study

We now consider the reaction of ethylene oxide (EO) with water to produce ethylene glycol (EG) in a reactive distillation column. The reaction is irreversible and proceeds in the presence of a catalyst

$$\mathrm{EtO} + \mathrm{H_2O} \rightarrow \mathrm{EG} \quad (9)$$

In addition we have an unwanted side reaction in which ethylene glycol reacts with ethylene oxide to di-ethylene-glycol (DEG).

$$\mathrm{EtO} + \mathrm{EG} \rightarrow \mathrm{DEG} \quad (10)$$

The reaction rate constant of the second reaction is, under reaction conditions, about three times as large as the rate constant of the first reaction. Therefore, in a conventional reactor with equimolar feed, a considerable amount of DEG is produced. Furthermore, the reactions are both highly exothermic requiring good temperature control. A reactive distillation column offers both the advantages of heat integration and in situ separation of the desired product, EG, preventing further reaction to DEG. By choosing total reflux operation, one can ensure that water mole fraction in the liquid phase on all the trays in the reactive section is close to unity (EO is considerably more volatile than water). The ethylene oxide that is supplied to the column reacts water to form EG and because of the high surplus of water in the liquid, the concentrations of ethylene oxide and ethylene glycol will be very low. This results in a low production rate of DEG. Furthermore, the distillation process provides direct temperature control, since the temperature of the liquid phases will always be at boiling point. Hot spot formation and the danger of runaway reactions are nonexistent in reactive distillation.

The column configuration chosen for the EG production is similar to the set-up of Ciric et al. [9,10], details of which are given in Fig. 8. This is a 10-stage sieve tray column (including total condenser and partial reboiler). Water is supplied to the top of the column, while the EO feed is distributed along the top section of the column. The column is operated at total reflux, while in the bottom a boilup ratio of 24 is maintained. The reaction kinetics and thermodynamics data are the same as those reported in the papers by Ciric and Miao [10] used an EQ model with homotopy continuation method to prove the existence of multiple steady states in the proposed set-up. We have carried out simulations with both the EQ and NEQ models. In both the EQ and NEQ model calculations, the condenser (stage 1) and the reboiler (stage 10) are modelled as equilibrium stages. Since the NEQ model calculations require the estimation of heat and mass transfer coefficients, we need to specify the tray configuration and layout. Four different sieve tray column configurations, with

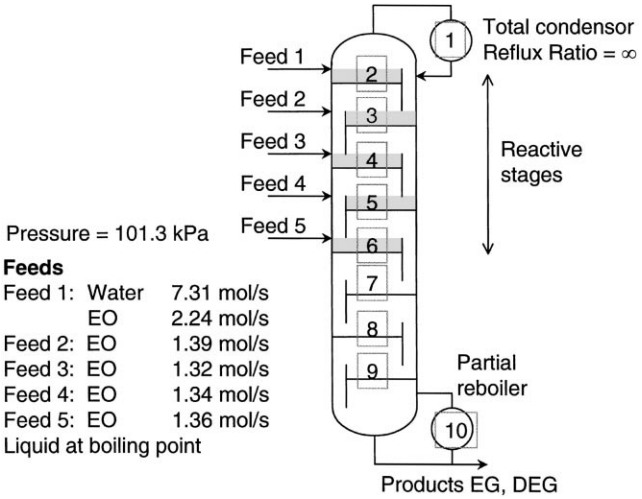

Fig. 8. Configuration of reactive distillation column for hydration of ethylene oxide to ethylene glycol. Further details to be found in [10].

column diameters of 1.7 and 3.0 m, were chosen for stages 2–9; these are specified in Table 3. Reactions are assumed to take place only on stages 2–6 because catalyst is considered to be present only on these stages. In the NEQ model calculations, the vapour and liquid phases were both assumed to be well-mixed on the given stage; this assumption was later relaxed to account for plug flow of both phases. To compare our results with those of Ciric and Miao [10] we also performed calculations with the EQ model.

Let us first consider the simulation results with the EQ model. These simulations, which are necessarily identical for all sieve tray configurations (cf. Table 3), are shown in Fig. 9. Three steady states SS-1 (high conversion), SS-2 (intermediate conversion) and SS-3 (low conversion) were found. The desired high conversion steady state solution (SS-1) corresponds to high column temperatures (cf. Fig. 9(b)) and lowest molar flow rate of the vapour up the column (cf. Fig. 9(c)). At first sight, it may appear counter-intuitive that the high conversion steady-state corresponds to the solution, which yields the smallest molar flows in the column.

Table 3
Sieve tray specification for ethylene glycol reactive distillation column

	Configuration 1	Configuration 2	Configuration 3	Configuration 4	Configuration 5
Type of tray	Sieve	Sieve	Sieve	Sieve	Sieve
Column diameter (m)	1.7	3.0	1.7	1.7	1.7
Total tray area (m^2)	2.27	7.07	0.67	2.27	2.27
Number of liquid flow passes	1	1	2	1	1
Tray spacing (m)	0.7	0.7	0.7	0.7	0.7
Liquid flow path length (m)	1.28	2.26	0.67	1.28	1.28
Active area/total tray area	0.86	0.86	0.86	0.86	0.86
Hole diameter (m)	0.0045	0.0045	0.0045	0.0045	0.0045
Total hole area/total tray area	0.0858	0.0858	0.0858	0.0858	0.0858
Downcomer area/total tray area	0.07	0.07	0.07	0.07	0.07
Weir length (m)	1.52	2.68	2.9	1.52	1.52
Weir length/column diameter	0.895	0.895	0.895	0.895	0.895
Weir height (m)	0.08	0.08	0.08	0.05	0.10
Downcomer clearance (m)	0.01	0.01	0.01	0.01	0.01

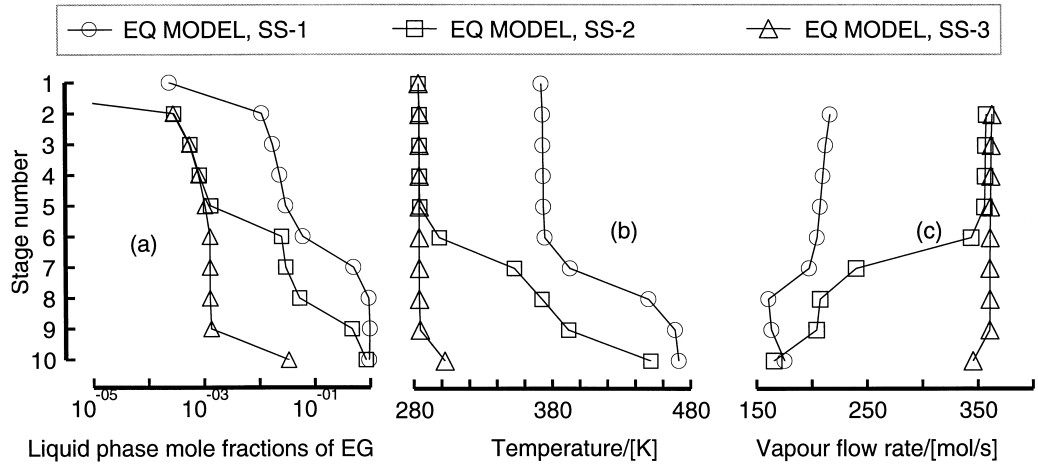

Fig. 9. Equilibrium model calculations for the ethylene glycol process. Column profiles for (a) liquid phase mole fraction, (b) temperature and (c) vapour phase molar flow.

Table 4
Steady-states for ethylene glycol column, using EQ model

	SS-1	SS-2	SS-3
Ethylene glycol mole fraction at bottom of column	0.9500	0.8446	0.0403
Heat duty of condenser (J)	-8.8×10^6	-9.6×10^6	-9.2×10^6
Heat duty of reboiler (J)	8.4×10^6	9.1×10^6	9.1×10^6
Temperature of reboiler (K)	471	451	302
Molar product flow at bottom of column ($\mathrm{mol\,s^{-1}}$)	7.3	7.3	14.2
Mass product flow at bottom of column ($\mathrm{kg\,s^{-1}}$)	0.47	0.47	0.47

In order to understand what is happening we have listed the important variables for the three steady-states in Table 4. We note that even though the molar flows in the three cases are widely different, the mass flow rate of the product leaving the column is identical for the three cases, as it should be in order to satisfy the overall column material balance. The reboiler duties in the three cases are nearly the same but not identical because of the difference is the molar heats of vaporisation of ethylene glycol and water.

Let us now consider the NEQ model simulations for the 1.7 m diameter column configuration. Again, three steady states were detected, high (SS-1), intermediate (SS-2) and low conversion (SS-3) of EO. For this chosen column diameter, only one solution, SS-1, can be realised in the column. The other solutions SS-2 and SS-3 could not be realised in the NEQ because for the higher vapour flows, the column floods in some (SS-2) or all (SS-3) of the stages; the flooding boundaries are drawn in Fig. 10(c).

For NEQ model simulations in the 3.0 m diameter column (configuration 2 of Table 3) we found the expected three steady states; see Fig. 11. The column diameter is, however, too large to accommodate the lower flows corresponding to SS-1 and SS-2. These lower vapour flows result in weeping on some (in case of SS-2) or all (in case of SS-1) of the trays; see Fig. 11(c). We therefore conclude that in the 3 m diameter column only the low conversion steady state can be realised.

The simulations presented in Figs. 9–11 were carried out assuming that on any tray the liquid and vapour phases are both well mixed. For modelling purposes the number of cells (cf. Fig. 3) used for each phase was equal to unity. For the 1.7 m diameter column calculations reported above, we had assumed that the liquid and vapour phases are both well mixed. With the NEQ cell model implementation (Fig. 3), we can study the influence of staging of the liquid and vapour phases by increasing the number of cells in either flowing phases. For five mixing cells in both vapour and liquid phases (which corresponds closely to plug flow conditions for either phase), the formation of by-product DEG is reduced while the conversion to EG is increased; see Fig. 12. Removing the mass transfer resistances, i.e. assuming the EQ model, gives the best performance with respect to conversion and selectivity; see the point towards the bottom right of Fig. 12.

We also carried out simulations to study the influence of tray hardware on conversion and selectivity and three variations of the base case configuration 1 were studied; these configurations (3,4 and 5) are specified in Table 3. For these simulations the number of mixing cells in the liquid and vapour phase were assumed to be equal to 1. The conversion to EG and to DEG are shown in Fig. 12. To understand the simulated values we need to have an understanding of the change in hydrodynamics with changing tray hardware. The important hydrodynamic and mass transfer parameters, plotted in Fig. 13 as a function of stage number are (a) liquid

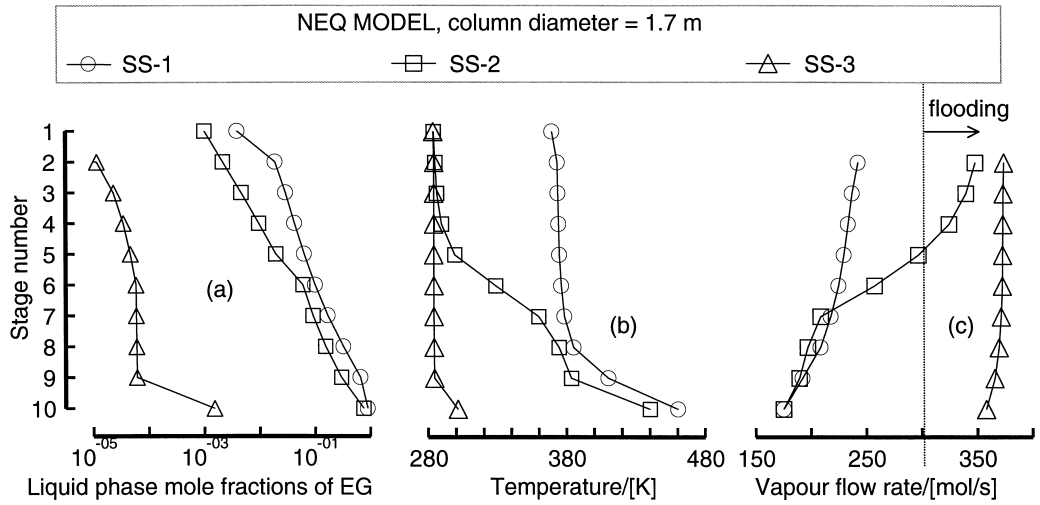

Fig. 10. Nonequilibrium model calculations for the ethylene glycol process for a column of diameter 1.7 m. Column profiles for (a) liquid phase mole fraction, (b) temperature and (c) vapour phase molar flow.

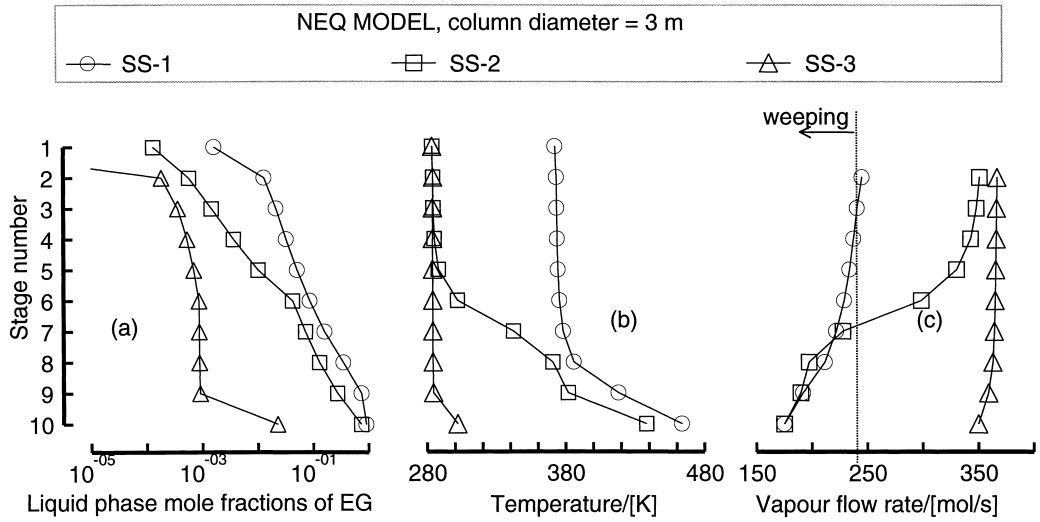

Fig. 11. Nonequilibrium model calculations for the ethylene glycol process for a column of diameter 3.0 m. Column profiles for (a) liquid phase mole fraction, (b) temperature and (c) vapour phase molar flow.

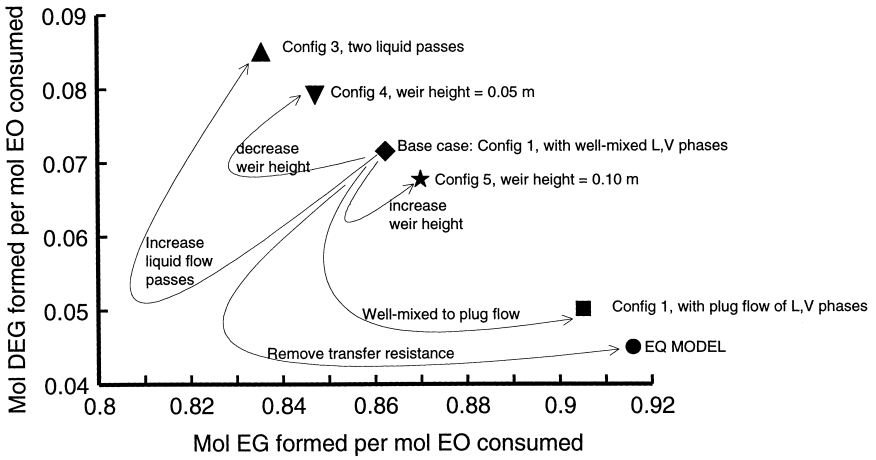

Fig. 12. Formation of by-product DEG vs. formation of EG for various tray configurations, specified in Table 3 and for various mixing model assumptions.

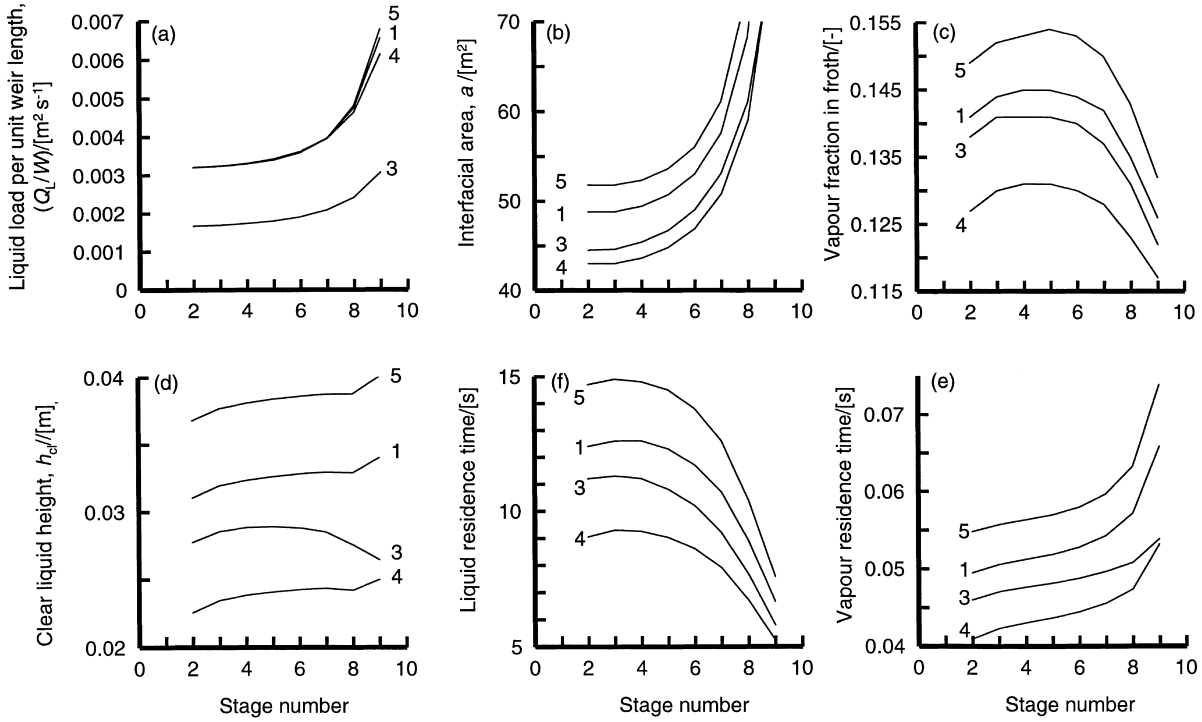

Fig. 13. Hydrodynamic and mass transfer parameters for various tray configurations 1, 3, 4 and 5 specified in Table 3.

load per unit weir length, Q_L/W, (b) total interfacial area on the tray, a, (c) vapour fraction in the froth on the tray (d) clear liquid height on the tray, h_{cl}, (e) liquid phase residence time on the tray and (f) vapour phase residence time on the tray.

Decreasing the weir height from 80 to 50 mm (changing from configuration 1–4 of Table 3) decreases formation of EG and increases by-product DEG formation; cf. Fig. 12. This reduction in performance is because the clear liquid height in configuration 4 is considerably lower than in the base case configuration 1 and the total interfacial area on the tray is reduced. The residence time of the vapour and liquid phases are also reduced. Mass transfer limitations are therefore increased in configuration 4, leading to lower conversion and selectivity. Increasing the weir height from 80 to 100 mm (changing from configuration 1 to configuration 5) leads to improved conversion and improved selectivity because of the exactly opposite effects as noted above in the change to configuration 4. High weir heights, and operation in the froth regime, are generally to be preferred in reactive distillation operations.

Consider the change in the performance when switching from Configuration 1 to 3 of Table 3 in which we have two liquid flow passes on the trays (for an explanation of single pass and multipass liquid flow configurations the reader is referred to the text of [36]). In this case the liquid load per weir length is reduced by 50%. This reduction in the liquid load leads to a reduction in the clear liquid height and lowering in the total interfacial area; see Fig. 13. Furthermore the liquid and vapour residence times are lower in the 2-pass configuration 3 when compared to the 1-pass configuration 1. All of this results in a lowering in the mass transfer rate, which has a detrimental influence on both the conversion and selectivity. It appears that the usual design rules for conventional distillation column design cannot be carried over to reactive distillation columns because, for a column of 1.7 m diameter the conventional design philosophy would be to use 2 passes for the liquid flow.

5. Concluding remarks

Comparison of the EQ and NEQ models for the MTBE and EG processes shows that the phenomena of multiple steady states has a much smaller realisable “window” if interphase mass and heat transfer resistances are taken into account. Some of the steady states found in the EQ model cannot be realised in the chosen column configuration because of flooding or weeping limitations.

The ethylene glycol case study was used to highlight the importance of hardware design on the performance of reactive distillation columns. While the EQ model anticipates three steady states, flooding and weeping considerations will ensure that only one steady state can be realised. Overdimensioning of the column will guarantee that only the low conversion steady state is realisable. The choice of weir height and number of passes has a significant influence on the conversion and selectivity.

It is concluded that for design of reactive distillation columns we must routinely resort to nonequilibrium stage modelling.

Acknowledgements

Partial support for our work comes from BP-Amoco Chemicals and Hyprotech Inc.

References

[1] A.A. Abufares, P.L. Douglas, Mathematical modeling and simulation of an MTBE catalytic distillation process using SPEEDUP and AspenPlus, Chem. Eng. Res. Des., Trans. Instn. Chem. Engrs, Part A 73 (1995) 3–12.
[2] V.H. Agreda, L.R. Partin, W.H. Heise, High-purity methyl acetate via reactive distillation, Chem. Eng. Progr. 2 (1990) 40–46.
[3] K. Alejski, J. Szymanowski, M. Bogacki, The application of a minimization method for solving reactive distillation problems, Comput. Chem. Eng. 12 (1988) 833–839.
[4] H.-J. Bart, H. Landschützer, Heterogene Reaktivdestillation mit axialer Rückvermischung, Chem. Ing. Tech. 68 (1996) 944–946.
[5] D.L. Bennett, H.J. Grimm, Eddy diffusivity for distillation sieve trays, AIChE J. 37 (1991) 589–596.
[6] J.L. Bravo, A. Pyhalathi, H. Jaervelin, Investigations in a catalytic distillation pilot plant: vapour/liquid equilibrium, kinetics, kinetics and mass transfer issues, Ind. Eng. Chem. Res. 32 (1993) 2220–2225.
[7] S. Carra, M. Morbidelli, E. Santacesaria, G. Buzzi, Synthesis of propylene oxide from propylene chlorohydrins. II. Modeling of the distillation with chemical reaction unit, Chem. Eng. Sci. 34 (1979) 1133–1140.
[8] S. Carra, E. Santacesaria, M. Morbidelli, L. Cavalli, Synthesis of propylene oxide from propylene-chlorohydrins. I. Kinetic aspects of the process, Chem. Eng. Sci. 34 (1979) 1123–1132.
[9] A.R. Ciric, D. Gu, Synthesis of nonequilibrium reactive distillation by MINLP optimization, AIChE J. 40 (1994) 1479–1487.
[10] A.R. Ciric, P. Miao, Steady state multiplicities in an ethylene glycol reactive distillation column, Ind. Eng. Chem. Res. 33 (1994) 2738–2748.
[11] R.P. Danner, T.E. Daubert, Manual for Predicting Chemical Process Design Data, AIChE, New York, 1983.
[12] J.L. DeGarmo, V.N. Parulekar, V. Pinjala, Consider reactive distillation, Chem. Eng. Progr. 3 (1992) 43–50.
[13] M.F. Doherty, G. Buzad, Reactive distillation by design, Chem. Eng. Res. Des., Trans. Instn. Chem. Engrs, Part A 70 (1992) 448–458.
[14] H.S. Eldarsi, P.L. Douglas, Methyl-tert-butyl ether catalytic distillation column. Part I: multiple steady states, Chem. Eng. Res. Des., Trans. Instn. Chem. Engrs, Part A 76 (1998) 509–516.
[15] J. Ellenberger, R. Krishna, Counter-current operation of structured catalytically packed distillation columns: pressure drop, holdup and mixing, Chem. Eng. Sci. 54 (1999) 1339–1345.
[16] J. Espinoza, E. Martinez, G.A. Perez, Dynamic behavior of reactive distillation columns, equilibrium systems, Chem. Eng. Commun. 128 (1994) 19–42.
[17] J.R. Fair, Design aspects for reactive distillation — columns for simultaneous reaction and separation need skillful planning, Chem. Eng. (New York) 105(11) (1998) 158.
[18] J.R. Fair, D.E. Steinmeyer, W.R. Penney, B.B. Croker, Gas absorption and gas–liquid system design, in: D.W. Green, J.O. Maloney (Eds.), Perry's Chemical Engineers' Handbook, Section 14, 7th ed., McGraw-Hill, New York, 1997.
[19] J.H. Grosser, M.F. Doherty, M.F. Malone, Modeling of reactive distillation systems, Ind. Chem. Eng. Res. 26 (1987) 983–989.
[20] T.E. Güttinger, M. Morari, Predicting multiple steady states in equilibrium reactive distillation. 1. Analysis of nonhybrid systems, Ind. Chem. Eng. Res. 38 (1999) 1633–1648.
[21] T.E. Güttinger, M. Morari, Predicting multiple steady states in equilibrium reactive distillation. 2. Analysis of hybrid systems, Ind. Chem. Eng. Res. 38 (1999) 1649–1665.
[22] S. Hauan, T. Hertzberg, K.M. Lien, Why Methyl-tert-butyl-ether production by reactive distillation may yield multiple solutions, Ind. Chem. Eng. Res. 34 (1995) 987–991.
[23] A.P. Higler, R. Taylor, R. Krishna, Modeling of a reactive separation process using a nonequilibrium stage model, Comput. Chem. Eng. 22, Supplement (1998) S111–S118.
[24] A. Higler, R. Taylor, R. Krishna, Nonequilibrium modelling of reactive distillation: multiple steady states in MTBE synthesis, Chem. Eng. Sci. 54 (1999) 1389–1395.
[25] A.P. Higler, R. Taylor, R. Krishna, The influence of mass transfer and liquid mixing on the performance of reactive distillation tray column, Chem. Eng. Sci. 54 (1999) 2879–2887.
[26] A. Higler, R. Krishna, J. Ellenberger, R. Taylor, Counter-current operation of a structured catalytically packed bed reactor: liquid phase mixing and mass transfer, Chem. Eng. Sci. 54 (1999) 5145–5152.
[27] R. Jacobs, R. Krishna, Multiple solutions in reactive distillation for methyl-tert-butyl ether synthesis, Ind. Eng. Chem. Res. 32 (1993) 1706–1709.
[28] H.A. Kooijman, Dynamic nonequilibrium column simulation, Ph.D. Dissertation, Clarkson University, Potsdam, USA, 1995.
[29] L.U. Kreul, A. Gorak, C. Dittrich, P.I. Barton, Dynamic catalytic distillation: advanced simulation and experimental validation, Comput. Chem. Eng. 22 (1998) S371–S378.
[30] R. Krishna, S.T. Sie, Strategies for multiphase reactor selection, Chem.Eng. Sci. 49 (1994) 4029–4065.
[31] R. Krishna, J.A. Wesselingh, The Maxwell–Stefan approach to mass transfer, Chem. Eng. Sci. 52 (1997) 861–911.
[32] R. Krishnamurthy, R. Taylor, Nonequilibrium stage model of multicomponent separation processes, AIChE J. 32 (1985) 449–465.
[33] M. Kubicek, Algorithm 502, dependence of a solution of nonlinear systems on a parameter, ACM Trans. Math. Softw. 2 (1976) 98–107.
[34] A. Kumar, P. Daoutidis, Modeling, analysis, analysis and control of ethylene glycol reactive distillation column, AIChE J. 45 (1999) 51–68.
[35] J.H. Lee, M.P. Dudukovic, A comparison of the equilibrium and nonequilibrium models for a multicomponent reactive distillation column, Comput. Chem. Eng. 23 (1998) 159–172.
[36] M.J. Lockett, Distillation Tray Fundamentals, Cambridge University Press, Cambridge, UK, 1986.
[37] K.D. Mohl, A. Kienle, E.D. Gilles, P. Rapmund, K. Sundmacher, U. Hoffmann, Steady-state multiplicities in reactive distillation columns for the production of fuel ethers MTBE and TAME: theoretical analysis and experimental verification, Chem. Eng. Sci. 54 (1999) 1029–1043.
[38] S.A. Nijhuis, F.P.J.M. Kerkhof, A.N.S. Mak, Multiple steady states during reactive distillation of methyl-tert-butyl-ether, Ind. Eng. Chem. Res. 32 (1993) 2767–2774.
[39] K. Onda, H. Takeuchi, Y. Okumoto, Mass transfer coefficients between gas and liquid phases in packed columns, J. Chem. Eng. Jpn. 1 (1968) 56–62.
[40] P.A. Pilavachi, M. Schenk, E. Perez-Cisneros, R. Gani, Modeling and simulation of reactive distillation operations, Ind. Eng. Chem. Res. 36 (1997) 3188–3197.
[41] P. Rapmund, K. Sundmacher, U. Hoffmann, Multiple steady states in a reactive distillation column for the production of the fuel ether TAME part II: experimental validation, Chem. Eng.Technol. 21 (1998) 136–139.
[42] A. Rehfinger, U. Hoffmann, Kinetics of methyl-tert-butyl ether liquid phase synthesis catalyzed by ion exchange resin. I. Intrinsic rate expression in liquid phase activities, Chem. Eng. Sci. 45 (1990) 1605–1616.
[43] A. Rehfinger, U. Hoffmann, Kinetics of methyl-tert-butyl ether liquid phase synthesis catalyzed by ion exchange resin. II. Macropore diffusion of MeOH as rate controlling step, Chem. Eng. Sci. 45 (1990) 1619–1626.
[44] R.C. Reid, J.M. Prausnitz, B.M. Poling, The Properties of Gases and Liquids, 4th ed., McGraw-Hill, New York, 1988.

[45] C.A. Ruiz, M.S. Basualdo, N.J. Scenna, Reactive distillation dynamic simulation, Chem. Eng. Res. Des., Trans. Instn. Chem. Engrs, Part A 73 (1995) 363–378.
[46] H. Sawistowski, P.A. Pilavakis, Distillation with chemical reaction in a packed column, Instn. Chem. Engrs Symp. Ser. No. 56, 1979, pp. 49–63.
[47] N.J. Scenna, C.A. Ruiz, S.J. Benz, Dynamic simulation of startup procedures of reactive distillation columns, Comput. Chem. Eng. 22 (1998) S719–S722.
[48] S. Schrans, S. de Wolf, R. Baur, Dynamic simulation of reactive distillation. An MTBE case study, Comput. Chem. Eng. 20 (1996) S1619–S1624.
[49] J.D. Seader, E.J. Henley, Separation Process Principles, Wiley, New York, 1998.
[50] J.D. Shoemaker, E.M. Jones, Cumene by catalytic distillation, Hydrocarbon Process. (1987) 57, 58.
[51] J.J. Siirola, An industrial perspective on process synthesis, AIChE Symp. Ser. No. 304, 91 (1995) 222–233.
[52] J. Simandl, W.Y. Svrcek, Extension of the simultaneous solution and inside–outside algorithms to distillation with chemical reactions, Comput. Chem. Eng. 15 (1991) 337–348.
[53] K. Sundmacher, Reaktivdestillation mit katalytischen fuel-lkoerperpackungen — ein neuer Process zur Herstellung der Kraftstoffkomponente MTBE, Ph.D Thesis, Universität Clausthal, 1995.
[54] K. Sundmacher, U. Hoffmann, Multicomponent mass transfer and energy transport on different length scales in a packed reactive distillation column for heterogeneously catalyzed fuel ether production, Chem. Eng. Sci. 49 (1994) 4443–4464.
[55] K. Sundmacher, Development of a new catalytic distillation process for fuel ethers via a detailed nonequilibrium model, Chem. Eng. Sci. 51 (1996) 2359–2368.
[56] K. Sundmacher, G. Uhde, U. Hoffmann, Multiple reactions in catalytic distillation processes for the production of the fuel oxygenates MTBE and TAME: analysis by rigorous model and experimental validation, Chem. Eng. Sci. 54 (1999) 2839–2847.
[57] R. Taylor, H.A. Kooijman, J.S. Hung, A second generation nonequilibrium model for computer simulation of multicomponent separation processes, Comput. Chem. Eng. 18 (1994) 205–217.
[58] R. Taylor, R. Krishna, Multicomponent Mass Transfer, Wiley, New York, 1993.
[59] T.L. Wayburn, J.D. Seader, Homotopy continuation methods for computer aided process design, Comput. Chem. Eng. 11 (1987) 7–25.
[60] X. Xu, Z. Zhao, S.-J. Tian, Study on catalytic distillation processes. Part III. Prediction of pressure drop and holdup in catalyst bed, Chem. Eng. Res. Des., Trans. Instn. Chem. Engrs, Part A 75 (1997) 625–629.
[61] Y. Zheng, X. Xu, Study on catalytic distillation processes. Part II. Simulation of catalytic distillation processes, quasi homogeneous rate based model, Chem. Eng. Res. Des., Trans. Instn. Chem. Engrs, Part A 70 (1992) 465–470.
[62] F.J. Zuiderweg, Sieve trays — a view on the state of art, Chem. Eng. Sci. 37 (1982) 1441–1461.